MULTISCALE MODELING OF HVOF THERMAL SPRAY PROCESS [1]

Mingheng Li and Panagiotis D. Christofides [2]

Department of Chemical Engineering
University of California, Los Angeles, CA 90095

Abstract: The major physicochemical processes involved in an industrial HVOF thermal spray process (Diamond Jet hybrid gun, Sulzer Metco, Westbury, NY) are studied by a comprehensive multiscale model. The model includes continuum type differential equations that describe the dynamics of gas phase and particles of different sizes, and a rule-based stochastic simulator that predicts the evolution of coating microstructure. On the macroscopic gas/particle dynamics side, the Favre-averaged Navier-Stokes equations and energy balance equations are solved with the renormalization group (RNG) k-ϵ turbulence model, and the particle trajectories, temperature histories and melting degrees are determined using the 4th order Runge-Kutta method. On the microscopic particle deposition side, the formation of coating microstructure is captured by certain rules that encapsulate the main physical features of particle deposition, deformation, solidification and coating growth. Parametric analysis based on the developed multiscale model is carried out to study the relationship between the macroscopic operating conditions and the particle in-flight behavior as well as the resulting coating microstructure.

Keywords: multiscale modeling, thermal spray, coating microstructure.

1. INTRODUCTION

Currently, there is a great interest in the field of nanostructured materials, whose grain sizes are typically less than 100 *nm* (Cheng *et al.*, 2003). This interest is motivated by the discovery that such materials have properties superior to those of conventional bulk materials including greater strength, hardness, ductility and sinterability, size-dependent light absorption, greater reactivity, etc. With the prompt advances in the production of high quality nanoscale powders, the focus of nanostructured materials research is now shifting from synthesis to processing, for example, the fabrication of nanostructured coatings using the so-called High Velocity Oxygen-Fuel (HVOF) thermal spray process (Ajdelsztajn *et al.*, 2002). The nanostructured coatings are widely used in many industries as thermal-barrier, wear-resistant and corrosion-protective surface layers to extend product life, to increase performance and to reduce production and maintenance costs.

In the HVOF thermal spray process, fine powder particles are heated and accelerated in a reacting gas flame and subsequently hit the substrate in a molten or semi-molten state, forming a thin layer of coating as a result of the solidification and sintering of the sprayed particles. In this work, we focus on modeling and control relevant analysis of the main physicochemical phenomena

[1] Financial support for this work from a 2001 ONR Young Investigator Award is gratefully acknowledged.
[2] Corresponding Author. Tel: +1-310-794-1015. Fax: +1-310-794-1015. Email: pdc@seas.ucla.edu.

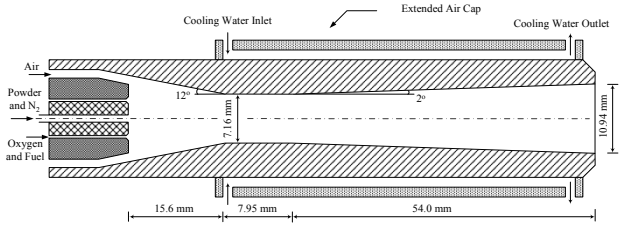

Fig. 1. Schematic diagram of the Diamond Jet hybrid thermal spray gun.

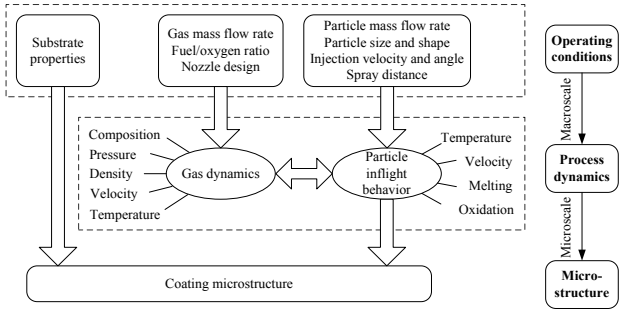

Fig. 2. Multiscale character of the HVOF thermal spray process.

involved within the industrial Diamond Jet hybrid HVOF thermal spray process, using a comprehensive multiscale model. The model will capture macroscopic gas dynamics and particle in-flight behavior as well as the microscopic deposition and coating microstructure evolution. Based on the proposed model, a control relevant parametric analysis is carried out to study the influence of key process parameters on the particle in-flight behavior and the resulting coating microstructure.

2. MULTISCALE MODELING OF THE HVOF THERMAL SPRAY PROCESS

2.1 Fluid and particle dynamics

Figure 1 shows a schematic diagram of the industrial Diamond Jet hybrid HVOF thermal spray process. A multiscale feature of the HVOF thermal spray process is shown in Figure 2 (Li *et al.*, 2004). In the HVOF thermal spray process, in order to transfer kinetic energy as much as possible to the particulate phase from the gas phase, the flow is usually maintained at supersonic conditions through a convergent divergent nozzle. To determine this supersonic compressible flow, the Favre-averaged Navier-Stokes equations and energy balance equations are solved with the renormalization group (RNG) k-ϵ turbulence model. The eddy dissipation model, which assumes that reactions occur infinitely fast and the reaction rate is limited by the turbulent mixing rate of fuel and oxidant, is employed here. In many practical situations like the HVOF thermal spray process, the eddy-dissipation model describes the limiting rate and thus a knowledge of accurate Arrhenius rate data, is not needed. This conclusion has been validated by experimental studies (Dolatabadi *et al.*, 2003). Based on the fact that the gas residence time in the combustion chamber (convergent section of the nozzle) is much longer than the subsequent parts, it is assumed that most of the reaction occurs in the chamber and the reaction moves forward following an equilibrium chemistry model. The detailed information is provided in a paper (Li and Christofides, 2005).

The particle trajectories, temperature histories and melting degrees are solved by a set of differential equations as follows:

$$\begin{aligned} m_p \frac{dv_p}{dt} &= \frac{1}{2} C_D \rho_g A_p (v_g - v_p)|v_g - v_p| \\ \frac{dx_p}{dt} &= v_p \\ m_p c_{p_p} \frac{dT_p}{dt} &= \begin{cases} hA'_p(T_g - T_p) + S_h \\ 0, \quad (T_p = T_m) \end{cases} \\ \Delta H_m m_p \frac{df_p}{dt} &= \begin{cases} hA'_p(T_g - T_p) + S_h \\ 0, \quad (T_p \neq T_m) \end{cases} \end{aligned} \tag{1}$$

where m_p is the mass of the particle, v_p is the axial velocity of the particle, t is the time, A_p is the projected area of the particle on the plane perpendicular to the flow direction, ρ_g is the density of the gas, C_D is the drag coefficient, and x_p is the position of the particle, T_p is the temperature of the particle, A'_p is the surface area of the particle, T_m is the melting point of the particle, ΔH_m is the enthalpy of melting and f_p is the ratio of the melted mass to the total mass of the particle ($0 \leq f_p \leq 1$). S_h is the source term including heat transfer due to radiation ($\varepsilon\sigma A'_p(T_g^4 - T_p^4)$) and oxidation. The heat transfer coefficient h is computed by the Ranz-Marshall empirical equation. Since the gas properties, such as temperature, velocity, and viscosity are all functions of x_p, the above equations can be solved by the 4th order Runge-Kutta method provided that the gas fluid/thermal field is known. Note that in the HVOF thermal spray processing of particles consisting of carbides with binding metals, such as the WC-Co powders used in this work, only the latter may experience a molten state because the gas temperature in a conventional HVOF thermal spray process is not high enough to melt the carbides. In such a case, the particle melting equation in Eq.1 is modified such that only the fusion of metals might occur in the gas thermal field. In the present work, the melting degree of particles represents the one of the binder (Cobalt) instead of the whole particulate phase.

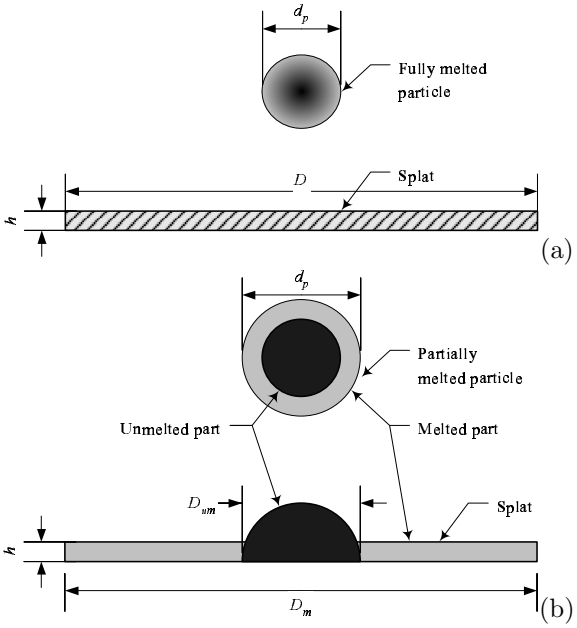

Fig. 3. Particle deformation - (a) fully melted, (b) partially melted.

2.2 Coating microstructure evolution

The thermally sprayed coating consists of lamellar splats interspersed with pores. The splats are the fundamental building blocks of the coating formed by the impact, deformation, spreading and solidification of individual droplets and the pores result from the interaction of the droplets and the previously deposited coating surface. In the simulation of coating microstructure evolution, it is assumed that the coating formation process is a sequence of independent discrete events of each individual particle hitting on the previously formed coating layer. In each event, a particle is randomly picked from a lognormally distributed size function, and its hitting point on the substrate is determined by two independent random variables. The velocity, temperature and degree of melting of this particle at the point of impact on the substrate will then be calculated based on the macroscopic model. As a result of deformation, the particle becomes a splat and is added onto the previously deposited coating surface according to certain rules as follows.

(1) Particle deformation follows Madejski model (Madejski, 1976). A fully melted particle becomes a thin cylinder as a result of deformation, and a partially particle becomes a semi-sphere around by a ring formed by the melted part.
(2) The melted part of a particle usually fits on the surface as much as possible.
(3) If the unmelted part of a partially melted particle hits at the point of the previously deposited layer that is formed by an unmelted particle, it will bounce off, and a hole will be formed in the center of the disk. Otherwise, it will attach on the coating surface as a hemisphere.
(4) If the splat comes to a vertical drop during spreading, the ratio of the splat that has not been settled down will be calculated. The splat may either cover a gap or break (or cover the corner) at the step, depending on the ratio and the height of the step.
(5) If the splat encounters a dead end, it will first fill the available space, and then flow over the outer surface, depending on the remaining volume.

A detailed discussion of the rule-based modeling of coating growth and coating microstructure was given in our previous work (Shi *et al.*, 2004).

3. RESULTS AND DISCUSSION

3.1 Analysis of Gas dynamics

The process model of gas dynamics was implemented into Fluent, a commercial CFD software, and was solved by finite volume method. The governing mass, momentum and energy balance equations together with the ideal gas state equation are solved at first using a first-order upwind scheme to get to a convergent solution and then a second-order upwind scheme to capture the shock diamonds that occur in the external flow field.The simulated contours and centerline profiles of static pressure, axial velocity and temperature in the internal and external fields are shown in Figure 4. In the combustion chamber (convergent section of the air cap), reaction of oxygen and propylene results in an increase of gas temperature to higher than 3000 K and a high pressure of 6 atm is maintained. As the exhaust gases expand the convergent-divergent nozzle, the pressure decreases and the gas velocity increases continuously. At the throat of the nozzle, the Mach number is around 1. The gas is accelerated to supersonic velocity in the divergent section of the nozzle, and reaches an average Mach number of 2 at the exit of the nozzle. Because the pressure at the exit of the nozzle is 0.6 atm, which is less than the atmospheric pressure, the flow outside of the gun is overexpanded and adjusts to the ambient pressure by a set of compression and expansion waves. The overexpanded flow condition gives a slightly higher gas velocity, and more kinetic energy can be transferred to the powders (Mills, 2003).

The solved particle in-flight behavior is shown in Figure 5. The profiles of gas velocity and temperature are also given in the same figure for reference. Note that as the plate is placed in the front of the gas flame, the gas will be stagnant at the point of

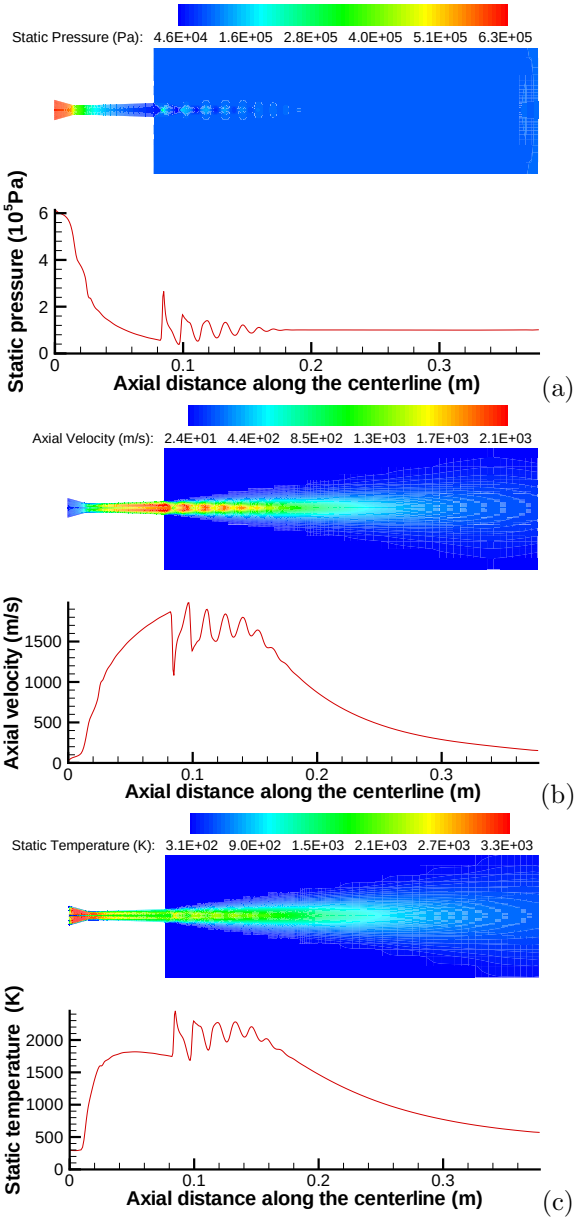

Fig. 4. Contours of flooded gas properties (upper plot) and centerline profiles of gas properties (lower plot) - (a) static pressure, (b) axial velocity, and (c) static temperature.

impact, i.e., its axial velocity is zero. It is shown that particles of small sizes may reach very high velocities during flight, however, their velocities drop more sharply than those of larger particles because of their smaller momentum inertias. For example, a particle with a diameter of 0.5 μm may reach a velocity of about 1800 m/s during flight, however, its velocity decays very sharply and it is eventually trapped by the gas stream. On the other hand, particles of small sizes may be heated to the melting point in a short time and be fully melted during flight, however, they may eventually be in a coexistence state of liquid and solid or even in a solid state after a long enough distance. Smaller particles tend to change their temperatures easily because of their smaller

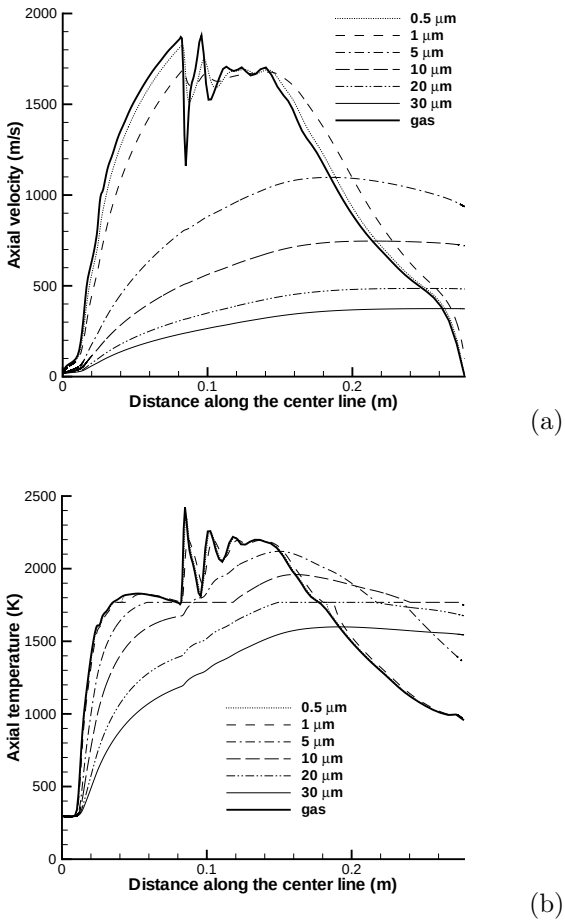

Fig. 5. Profiles of (a) particle velocity and (b) temperature along the centerline.

thermal inertias. The smaller the particle size is, the easier its temperature varies. For particles of large sizes, however, their period for acceleration and heating are both longer, and their velocity (or temperature) profiles become nearly flat as they approach the same velocity (or temperature) of the gas. Moreover, they may not reach the melting point and keep the solid state along the whole flow field. Particles of medium sizes, however, may become partially melted during flight.

Based on the proposed CFD model, a control relevant parametric analysis is performed to study the effect of gas flow rate on the gas dynamics, and the simulation results under different gas flow rates (see Table 1) are shown in Figure 6. It is important to note that the gas momentum flux ($\rho_g v_g^2$) is approximately proportional to the drag force (if the drag coefficient is assumed to be approximately constant) and the gas temperature, whose different between the particle temperature, provides the driving force for particle heating. We plotted the influence of gas flow rates on these two key parameters based on the simulation results in subsection 3.1 and the results are shown in Figure 7. It is clear that the momentum flux increases with the total mass flow rate. However, a higher

total mass flow rate does not imply a higher temperature. Rather, the gas temperature in the free jet is highly dependent on the fuel/oxygen ratio, although a higher total flow rate helps to maintain the potential core for a longer distance. For example, the total gas flow rate is the lowest in case 2. However, the particle temperature achieved in this case is even higher than the one in cases 1 and 3, which clearly show that the fuel/oxygen ratio is a key parameter that can be manipulated to adjust particle temperature and degree of melting. An optimal equivalence ratio (fuel/oxygen ratio divided by its stoichiometric value) of the propylene/oxygen system is determined to be around 1.2 (Li *et al.*, 2004). To precisely control particle velocity and melting ratio, the gas momentum flux and gas temperature should be adjusted independently through the regulation of the flow rate of each gas stream. The readers may refer to our previous work (Li *et al.*, 2004) for detailed discussions.

Table 1. Different operating conditions.

	C_3H_6 $(scfh)$	O_2 $(scfh)$	Air $(scfh)$	N_2 $(scfh)$	$\dot{m}$ (g/s)	φ
1	176	578	857	28.5	18.1	1.05
2	176	578	428	28.5	13.7	1.19
3	176	867	857	28.5	21.4	0.76
4	264	867	1286	28.5	27.0	1.05

case 1 is the baseline condition.

3.2 Analysis of coating microstructure evolution

In the simulation of coating microstructure evolution, the coating cross section that is perpendicular to the substrate is discretized using a 8192 $\times$ 4096 mesh. The size of each grid in the mesh is 0.1 $\times$ 0.1 μm. The particles are assumed to lognormally distributed with $d_{10} = 4$ μm, $d_{50} = 12$ μm, and $d_{90} = 36$ μm. (d_{10}, d_{50} and d_{90} are three characteristic diameters with the subscript representing the percentage of the finer particles in the sample than each characteristic diameter. For example, 10% of the sample is finer than d_{10}.) Figure 8 shows the simulated configuration of the coatings deposited under the first (baseline) and the forth conditions, respectively. In Figure 8(a), the particle melting ratio is low. As a result, many solid particles, especially those of large sizes bounce off the substrate, and the coating is mainly composed by small particles that are in a partially molten state. In this case, the he porosity is high (about 4.6%). However, when the particle melting ratio increases, both the unmelted particles or the unmelted part of partially melted particle have a high probability to be attached to the previous deposited coating instead of being bounced off. A high deposition efficiency and low coating porosity can still be achieved. This study shows that the coating microstructure is highly dependent on the

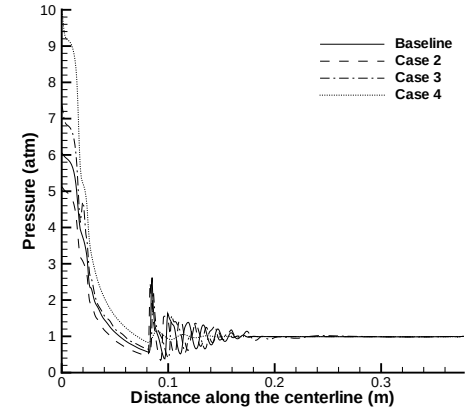

(a)

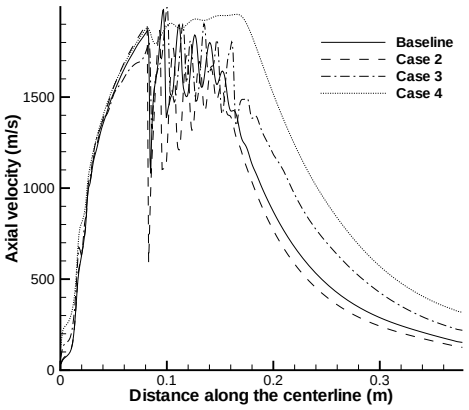

(b)

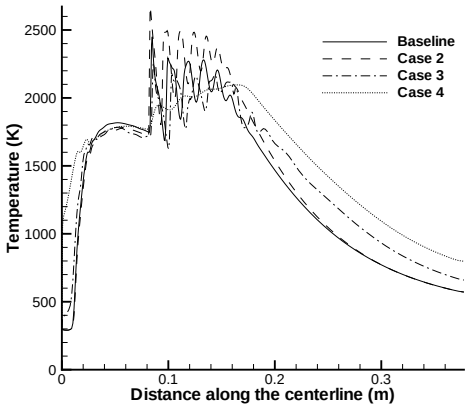

(c)

Fig. 6. Influence of gas flow rates on gas properties - (a) static pressure, (b) axial velocity, and (c) static temperature.

operating conditions and entails the implementation of real-time diagnosis and control.

4. CONCLUSION

A multiscale modeling framework of HVOF thermal spray process is developed and applied to the processing of WC-Co particles using a representative process. A particle laden supersonic reacting flow with overexpanded flow condition at the

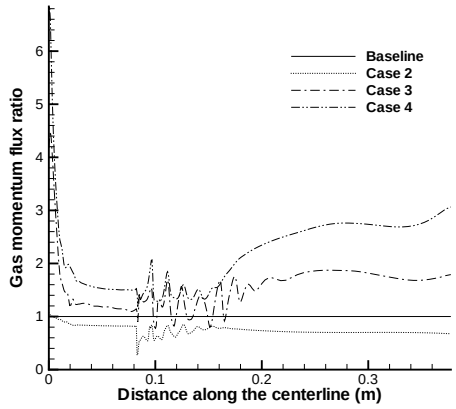

(a)

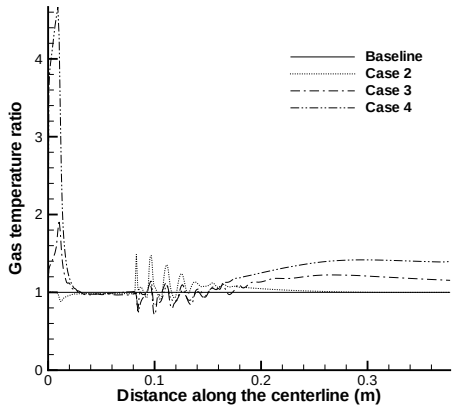

(b)

Fig. 7. (a) gas momentum flux, and (b) gas temperature along the centerline under different gas flow rates. Normalization is done with respect to the corresponding properties under baseline operating conditions.

exit of the nozzle is solved using CFD simulation and the formation of coating microstructure is captured by rule-based stochastic simulation. The simulation results show that coating microstructure is sensitive to particle state at the point of impact and motivate the precise control of the process parameters to suppress coating variability.

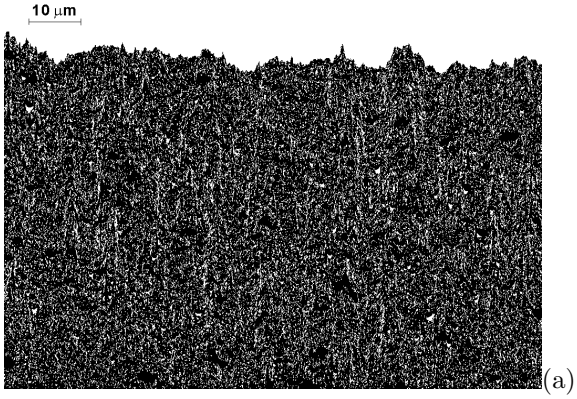

(a)

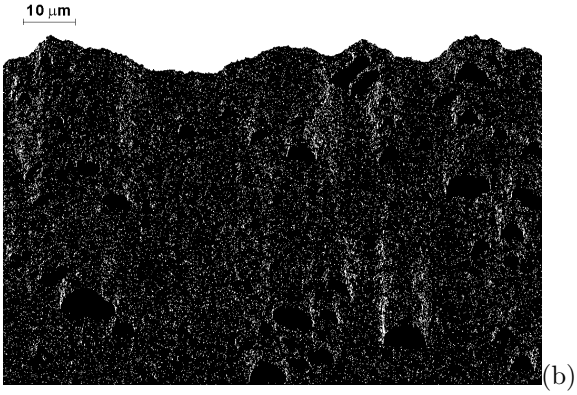

(b)

Fig. 8. Simulated coating microstructure under different operating conditions. (a) baseline and (b) case 4.

REFERENCES

Ajdelsztajn, L., J. Lee, K. Chung, F. L. Bastian and E. J. Lavernia (2002). Synthesis and nanoindentation study of high-velocity oxygen fuel thermal-sprayed nanocrystalline and near-nanocrystalline Ni coatings. *Metall. Mater. Trans. A* **33**, 647–655.

Cheng, D., G. Trapaga, J. W. McKelliget and E. J. Lavernia (2003). Mathematical modelling of high velocity oxygen fuel thermal spraying of nanocrystalline materials: an overview. *Modelling Simul. Mater. Sci. Eng.* **11**, R1–R31.

Dolatabadi, A., J. Mostaghimi and V. Pershin (2003). Effect of a cylindrical shroud on particle conditions in high velocity oxy-fuel spray process. *J. Mater. Process. Tech.* **137**, 214–224.

Li, M. and P. D. Christofides (2005). Multiscale modeling and analysis of HVOF thermal spray process. *Chem. Eng. Sci.* to appear.

Li, M., D. Shi and Christofides P. D. (2004). Diamond jet hybrid HVOF thermal spray: Gas-phase and particle behavior modeling and feedback control design. *Ind. & Eng. Chem. Res.* **43**, 3632–3652.

Madejski, J. (1976). Solidification of droplets on a cold surface. *Int. J. Heat Mass Transfer* **19**, 1009–1013.

Mills, D. (2003). Personal communication, Sulzer Metco.

Shi, D., M. Li and P. D. Christofides (2004). Diamond jet hybrid HVOF thermal spray: Rule-based modeling of coating microstructure. *Ind. & Eng. Chem. Res.* **43**, 3653–3665.